Published in AJSE, Vol: 25, Issue:1
Received on 15th March 2025
Revised on 13th August 2026
Published on 31st August 2026

AIUB JOURNAL OF SCIENCE AND ENGINEERING
ISSN: 1608 - 3679 (print) 2520 - 4890 (Online)
https://doi.org/10.53799/sxy06285

Influence of Different Road Vehicle Positioning on The Aerodynamic and Aeroacoustics Characteristics Using CFD Analysis

Nur Rasyidah Roziman, Izuan Amin Ishak, Mohammad Arafat, Nor Afzanizam Samiran, Nur Haziqah Shaharuddin, Fadhilah Mohd Sakri, Muhammad Aidil Safwan Abdul Aziz, Muhammad Nabil Farhan Kamal

***Abstract*—The rapid growth of private vehicle usage in urban corridors intensifies traffic congestion, driving up fuel consumption and vehicle emissions. This study evaluates how relative vehicle positioning and longitudinal spacing govern aerodynamic drag and aeroacoustic performance using computational fluid dynamics (CFD). Numerical simulations assess aerodynamic forces, surface pressure distributions, wake dynamics, and acoustic power generation for heterogeneous platoons comprising passenger cars and double-decker buses. Following grid-independence validation, six multi-vehicle configurations with 4 m and 8 m inter-vehicle gaps were evaluated. The Bus–Car–Car platoon with a 4 m gap (Case E) yielded the most pronounced drag reduction. Under this configuration, the lead bus drag coefficient (C_d) dropped to 0.671, while the trailing cars experienced substantial drag reductions, reaching C_d values of 0.148 and 0.246. Compared to baseline isolated models, Case E achieved up to a 37% drag reduction for the bus and a 50–60% reduction for the trailing passenger cars. This arrangement promotes rapid flow recovery and suppresses severe turbulence, thereby stabilizing downstream pressure fields and lowering acoustic power output. These findings offer practical insights into optimizing mixed-vehicle platoons to enhance transport efficiency and lower aerodynamic losses.**

***Index Terms*—Computational Fluid Dynamics (CFD), Vehicle Positioning, Longitudinal space, Aerodynamic Drag, Aeroacoustics Characteristics, Drag Coefficient, Lift Coefficient, Wake Interference, and Noise Reduction.**

I. INTRODUCTION

THE rapid growth of urban populations and economic wealth has led to an increase in private vehicle ownership. This rise in the number of vehicles has inevitably resulted in greater congestion, particularly during peak hours. This situation leads to increasing fuel consumption and pollution of the environment [1]. When vehicles travel closely together in convoys, it greatly influences the aerodynamic interactions between the vehicles and their overall performance. Vehicles with a short distance between them can decrease the aerodynamic drag because the vehicle in front is affected by the air pressure that occurs by the pushing force behind it. The vehicle close behind another is less affected by the aerodynamic drag due to the vehicle in front of it breaking the strong wind [2]. From this, it can be shown that when a vehicle travels in a convoy or a line, it can affect the aerodynamic flow of it.

Previous research [3] demonstrates that a vehicle's relative position dictates its surrounding airflow dynamics. During platooning, the lead vehicle carves out a low-pressure wake, effectively shielding trailing vehicles and reducing their aerodynamic drag. This effect is mainly due to drafting. This research by [4] also indicates that drag reduction is highly sensitive to the distance between vehicles (inter-vehicle spacing). A smaller gap reduces drag on trailing vehicles but can increase turbulence and pressure drag on the leading vehicle if improperly spaced. Similarly, longitudinal spacings influence drags by altering wake overlap and flow interference patterns. As shown in [5] research focuses on the effects of vehicle spacing on aerodynamic drag in truck platoons it shows that arranging two trucks in a platoon with 3 meters spacing reduces aerodynamic drag by about 36%. The trailing truck experiences just 63.3% of the drag of a solo truck. Even with a safe spacing of 6 meters, significant drag reductions highlight the advantages of optimal vehicle spacing for fuel efficiency. The research conducted by [6] and [7] also states that when the lorry is in platooning configurations, it significantly reduces the aerodynamic drag due to trailing lorries immersed in the turbulent flow created by the first lorry. Consequently, many studies investigate homogeneous platoons, primarily focusing on heavy-duty transport vehicles to optimize operational

Nur Rasyidah Roziman is a student at Universiti Tun Hussein Onn Malaysia, Muar, Johor, Malaysia (e-mail: an210102@student.uthm.edu.my)
Izuan Amin. Ishak is with the Department of Mechanical Engineering Technology, Universiti Tun Hussein Onn Malaysia, Pagoh Campus, Johor, Malaysia (e-mail: izuan.amin@gmail.com).
Mohammad Arafat is with Universiti Kuala Lumpur – Malaysian Institute of Aviation Technology (UniKL MIAT), Selangor, Malaysia (e-mail: arafat.mohammad@t.unikl.edu.my; marafatbd@gmail.com).
Nor Afzanizam Samiran is with the Department of Mechanical Engineering Technology, Universiti Tun Hussein Onn Malaysia, Pagoh Campus, Johor, Malaysia (e-mail: norafzanizam@uthm.edu.my).
Nur Haziqah Shaharuddin is a PhD student at Keio University, Yokohama, Japan (e-mail: haziqahshaharuddin@keio.jp).
Fadhilah Mohd Sakri is with the Taylor's University, School of Engineering, 1 Jalan Taylor's, 47500 Subang Jaya, Selangor, Malaysia (e-mail: Fadhilah.MohdSakri@taylors.edu.my).
Muhammad Aidil Safwan Abdul Aziz is a PhD student at the Department of Mechanical Engineering Technology, Universiti Tun Hussein Onn Malaysia, Pagoh Campus, Johor, Malaysia (e-mail: aidilsaf14@gmail.com)
Muhammad Nabil Farhan Kamal is a Project Engineer at Pentamaster Corporation, Persiaran Cassia Selatan 6, Taman Perindustrian Batu Kawan, Penang, Malaysia. (email: nabil.farhan.kamal@pentamaster.com.my)

efficiency and minimize fuel costs [8].

This research utilizes Computational Fluid Dynamics (CFD) simulations to investigate the aerodynamic and aeroacoustic performance of road vehicles across diverse configurations. This study evaluates how vehicle positioning and spacing alter aerodynamic loads, flow patterns, and acoustic power generation. Understanding these flow-field interactions is crucial for exposing structural limitations in modern vehicle design. By mapping these dynamics, this research provides practical insights for optimizing vehicle geometry and improving safety in dense traffic environments.

II. METHODOLOGY

A. Model Description

The vehicle models used in this study comprise a simplified SUV and a double-decker bus. As illustrated in Fig. 1, the geometric dimensions of the simplified SUV are 4.51 m in length, 1.765 m in width, and 1.675 m in height. For the double-decker bus, the representative dimensions are defined as 14 m in length, 2.6 m in width, and 4.1 m in height, as detailed in Fig. 2.

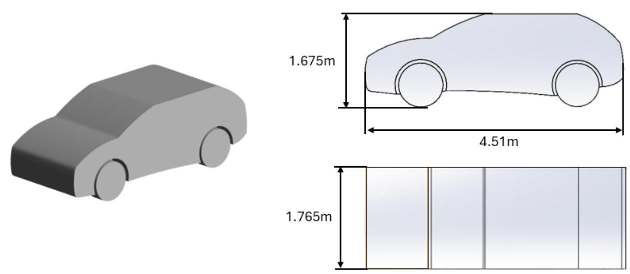

Fig. 1 Orthogonal views of the simplified car with dimensions

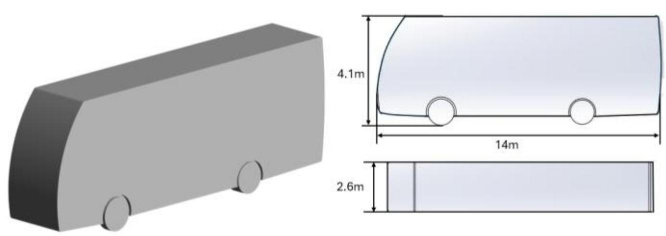

Fig. 2 Orthogonal views of the double-decker bus with dimensions

B. Enclosure and Boundary Conditions

To minimize blockage effects and prevent artificial boundary reflections, the computational fluid domain was generated using the enclosure tool within ANSYS based on vehicle characteristic dimensions, L = 14m, H = 4.1m, and W = 2.6m, resulting in a ($5L \times 4H \times 7W$) domain. The computational domain was designed to minimize blockage effects while maintaining computational efficiency. An upstream distance of *2L* and a downstream distance of *3L* were adopted following previously published numerical studies of external vehicle aerodynamics employing similar pressure-outlet boundary conditions [9], [10], [11]. These studies demonstrated that such domain dimensions provide accurate predictions of aerodynamic forces while maintaining reasonable computational cost. The simulation boundary conditions, illustrated in Fig. 3, feature a uniform velocity inlet of 20 m/s (corresponding to a Reynolds number $Re \approx 5.4 \times 10^6$) and a static gauge pressure outlet, with all vehicle surfaces defined as stationary no-slip walls [12].

.

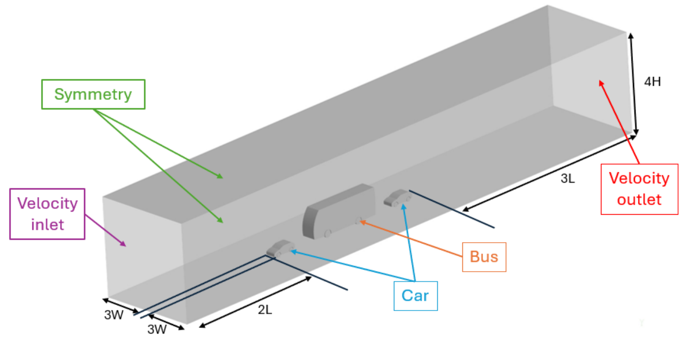

Fig. 3 Dimensions of the enclosure for the case and the name of the boundary are shown [10].

C. Meshing

A Poly-Hexacore mesh with a global baseline size of 0.032 m was used to discretize the computational domain. To properly capture the near-wall boundary layers, 10 inflation layers starting at a thickness of 1.0 mm were generated (see Figs 4 and 5)

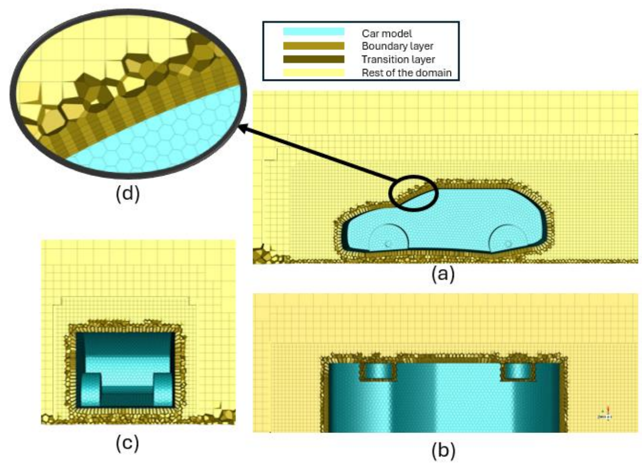

Fig. 4 Mesh generation of the car. View from: (a) side view, (b) top view, (c) front view, and (d) schematic grid layer near boundary

D. Simulation Setup

Once the computational mesh was generated, the numerical simulations were performed in ANSYS Fluent using the Standard k–ω turbulence model. The Standard k–ω model was selected for its superior near-wall flow prediction and robust handling of adverse pressure gradients compared to the Standard k–ε model [13]. These characteristics make it highly suitable for external bluff-body aerodynamics characterized by flow separation and complex wake interactions. Additionally, the model is widely adopted in vehicle aerodynamics studies due to its optimal balance between computational efficiency and predictive accuracy [14].

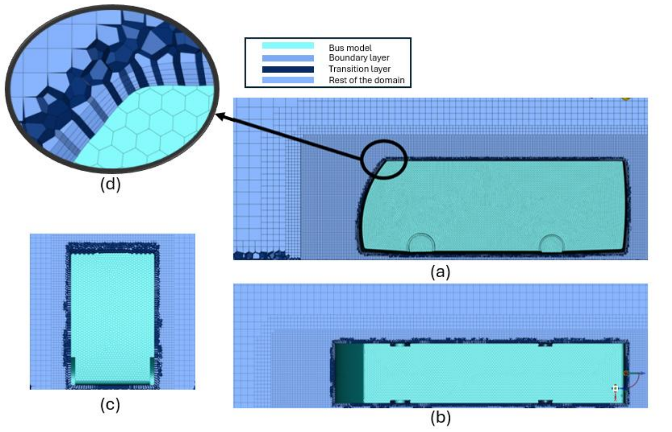

Fig. 5 Mesh generation of the bus. View from: (a) side view, (b) top view, (c) front view, and (d) schematic grid layer near boundary

Convergence was evaluated by monitoring residual trends alongside the drag coefficient, as depicted in Fig. 6. By 150 to 200 iterations, the momentum residuals had fallen to about 10^{-6} and turbulence metrics had stabilized. While severe flow separation kept the continuity residual somewhat higher, it showed no further decrease with additional iterations. With the drag coefficient flattening out near 160 iterations, steady-state convergence was established, making 500 iterations adequate for the aerodynamic calculations. However, broadband noise predictions required 2,000 iterations to fully stabilize the turbulence fields for accurate acoustic modeling.

E. Mesh Refinement

A grid independence test was carried out to verify the effect of spatial resolution on the simulation outcomes. By adjusting the global element size and refinement controls, three mesh densities were generated: coarse (Mesh 1), medium (Mesh 2), and fine (Mesh 3). The element counts and calculated aerodynamic forces for each setup are detailed in Table 1. Figure 8 compares the midplane velocity contours across these grids, revealing that while the coarse mesh blurs fine flow structures, the finer meshes accurately capture critical boundary layer details and local velocity gradients.

To assess the accuracy of the simulations, the drag coefficients (C_d) from each grid were compared. The medium grid (Mesh 2) resulted in a C_d of 0.72, showing a 7.69% deviation compared to Mesh 1.

The drag coefficient exhibits a monotonic convergence trend with mesh refinement, whereas the lift coefficient shows a larger variation, particularly for the finest mesh. Such behaviour is commonly observed in bluff-body aerodynamics because lift is more sensitive to local wake structures and pressure fluctuations than drag [15], [16], [17]. Considering that the difference in drag coefficient between Mesh 2 and Mesh 3 is only 2.78%, while the computational cost increases substantially for Mesh 3, Mesh 2 was selected as the optimal mesh for the subsequent simulations.

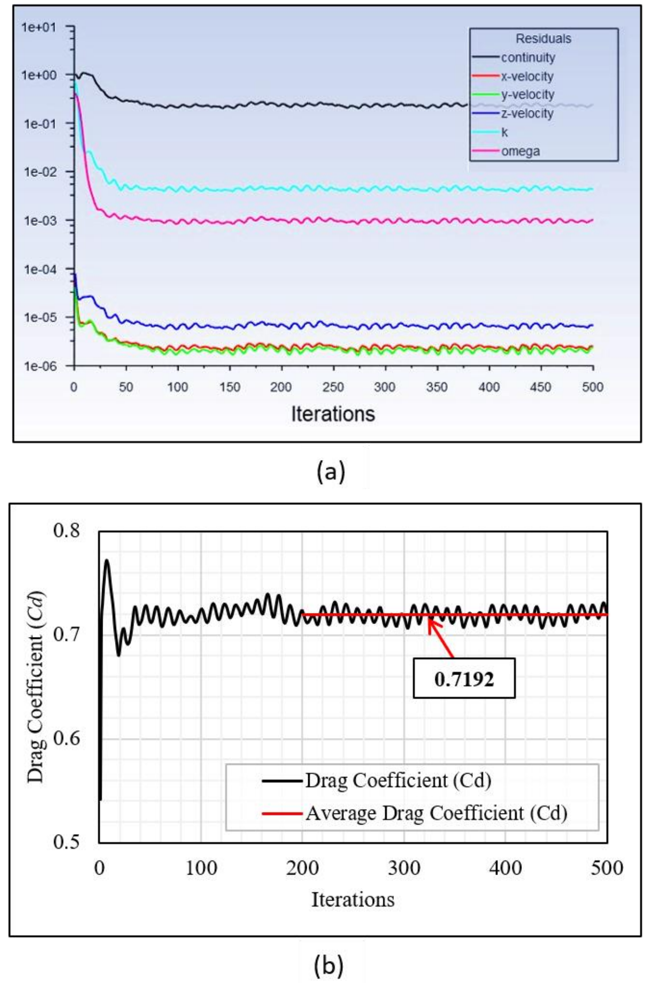

Fig. 6 Solution convergence for selected mesh; (a) residual plot, and (b) drag coefficient plot.

TABLE 1
PARAMETERS THAT ARE USED IN THE MESH REFINEMENT STUDY

Parameter	Mesh type		
	Mesh 1	Mesh 2	Mesh 3
Size of mesh (mm)	0.040	0.032	0.008
Number of Element (cell)	935,518	1,201,660	2,812,111
Number of Nodes	2,563,895	2,918,819	4,380,565
Drag Force Coefficient, C_d	0.78	0.72	0.70
Lift Force Coefficient, C_l	-0.134	-0.115	-0.222
Number of Iterations	500	500	500
Percentage difference (%)	-	7.69	2.78

Fig. 7 compares the midplane velocity contours for the coarse, medium, and fine grids. As expected, the fine grid (Mesh 3) clearly captures sharp velocity gradients and intricate boundary-layer details around the vehicle. In contrast, the coarse spatial resolution of Mesh 1 causes artificial numerical smoothing, blurring smaller flow features and underpredicting wake gradients. Moving from the coarsest to the finest mesh visibly reduces this artificial dissipation in the downstream flow.

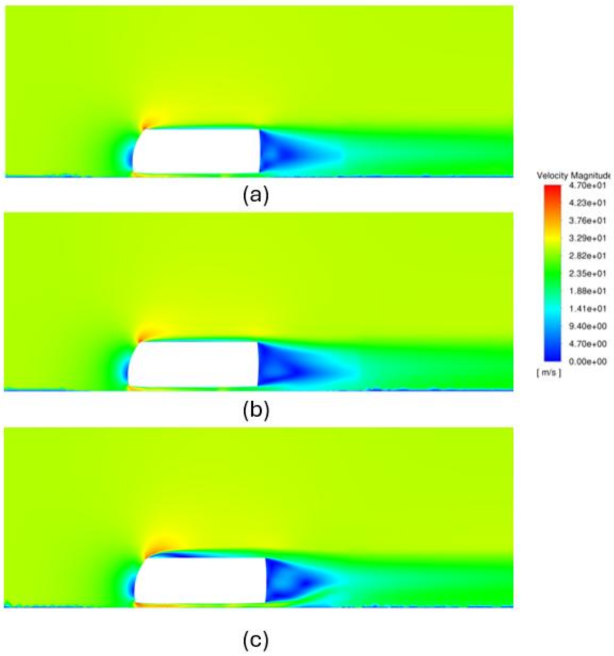

Fig. 7 *Velocity contour (a) Mesh 1, (b) Mesh 2, (c) Mesh 3*

F. Acoustic Modelling

Aeroacoustic characteristics were evaluated using the Broadband Noise Source Model available in ANSYS Fluent. The model estimates noise generation based on local turbulence quantities obtained from the RANS solution. The acoustic power generated by turbulent flow structures can be expressed as:

$$P_A \propto \rho \epsilon \left(\frac{u'}{c_0}\right)^5 \tag{1}$$

where P_A is the acoustic power, ρ is the fluid density, ϵ is the turbulence dissipation rate, u' is the turbulent velocity fluctuation, and c_0 is the speed of sound. Surface acoustic power distributions were used to identify regions of dominant noise generation associated with flow separation, vortex shedding, and wake interactions around the vehicles.

G. Case Details

To fully capture the aerodynamic and aeroacoustic dynamics, this study examines eight distinct vehicle configurations (summarized in Table 2). The core of the analysis focuses on three specific platooning sequences depicted in Fig. 8. We applied two inter-vehicle spacings, 4 m and 8 m to each sequence to assess the direct impact of physical proximity on wake interference. The remaining two cases evaluate a solitary car and a solitary bus, serving as control baselines for the multi-vehicle scenarios.

TABLE 2
SUMMARY OF ALL CASES

Case	Positions of road vehicles	longitudinal spacings
A	Car	-
B	Bus	-
C	Car-Bus-Car	4m
D	Car-Car-Bus	4m
E	Bus-Car-Car	4m
F	Car-Bus-Car	8m
G	Car-Car-Bus	8m
H	Bus-Car-Car	8m

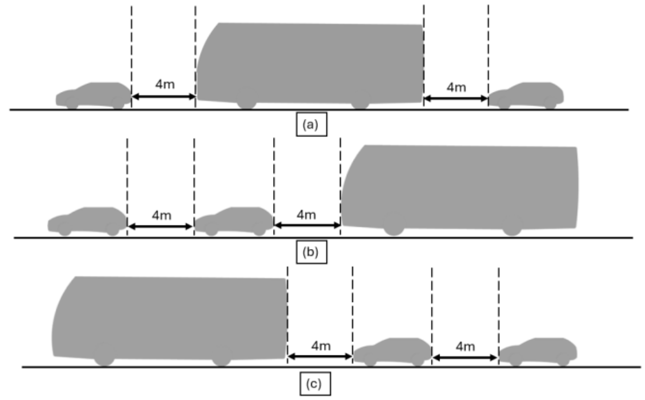

Fig. 8 Three different positions of road vehicles: (a) Car-Bus-Car, (b) Car-Car-Bus, (c) Bus-Car-Car.

III. RESULTS AND DISCUSSIONS

A. Aerodynamic analysis

Looking at the baseline simulations in Figure 9(a), the isolated car (Case A) maintains relatively smooth velocity streamlines. Flow separation is minimal, leaving only a tight, localized wake directly behind the vehicle. The bus (Case B), however, behaves entirely differently. Because of its bluff-body profile, it forces a high-pressure stagnation zone at the front and triggers severe flow separation. This creates a highly turbulent, expansive wake that thoroughly disrupts the downstream airflow.

For multi-vehicle configurations, as illustrated in Fig. 9(c)–9(h), the aerodynamic interactions vary significantly based on the vehicle arrangement and longitudinal space. In Case C, the Car-Bus-Car configuration with a 4 m longitudinal space shows strong interactions between the vehicles, dominated by the bus's wake, which increases turbulence and drag for the trailing car. In Case D, the Car-Car-Bus arrangement creates complex flow patterns as the wakes of the two leading cars combine and interact with the bus’s larger wake, leading to extensive downstream turbulence. Case E, featuring the Bus-Car-Car setup, shows the bus’s large wake significantly affecting both trailing cars, creating asymmetric flow fields and persistent vortex structures. The flow improves with an 8-meter longitudinal space due to reduced wake interference. In Case F, the Car-Bus-Car setup allows for better velocity recovery and reduced turbulence for the trailing car, though the bus’s wake remains dominant. In Case G, the Car-Car-Bus configuration benefits from improved wake dissipation for the leading cars, but the bus still generates a significant turbulent wake downstream. Finally, in Case H, the Bus-Car-Car arrangement achieves the most stable flow characteristics, with increased spacing reducing turbulence for the trailing cars and improving overall aerodynamic performance. These results underscore the influence of vehicle positioning and longitudinal spacing on wake interaction, turbulence intensity, and aerodynamic efficiency.

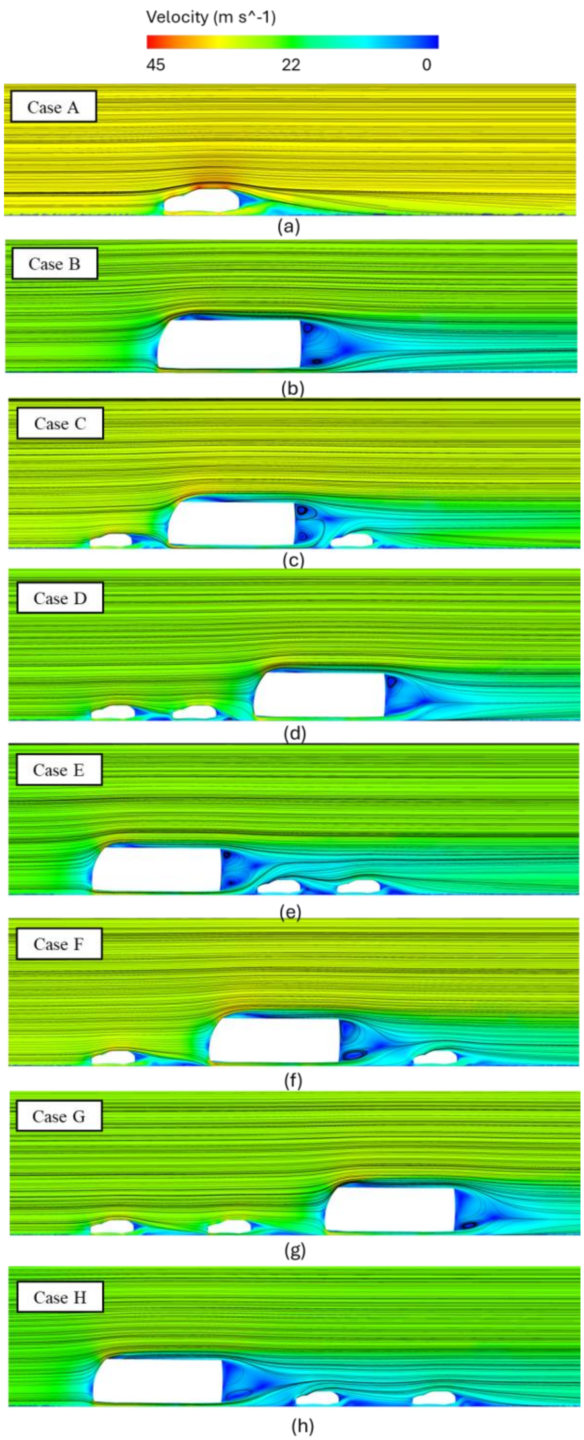

Fig. 9 Velocity streamline profiles for Case A, Case B, Case C, Case D, Case E, Case F, Case G and Case H

Fig. 10 illustrates the pressure distributions for Cases A–H, highlighting how vehicle arrangement and spacing influence aerodynamic performance. In Case C, the central positioning of the bus leads to a significant high-pressure zone at its front, which results in a large low-pressure wake that greatly increases drag and instability for the trailing car, even with a 4-meter longitudinal space. Case D shows that the combined wakes from the two leading vehicles create a low-pressure area that interacts with the bus's wake, resulting in uneven pressure distribution and increased turbulence downstream.

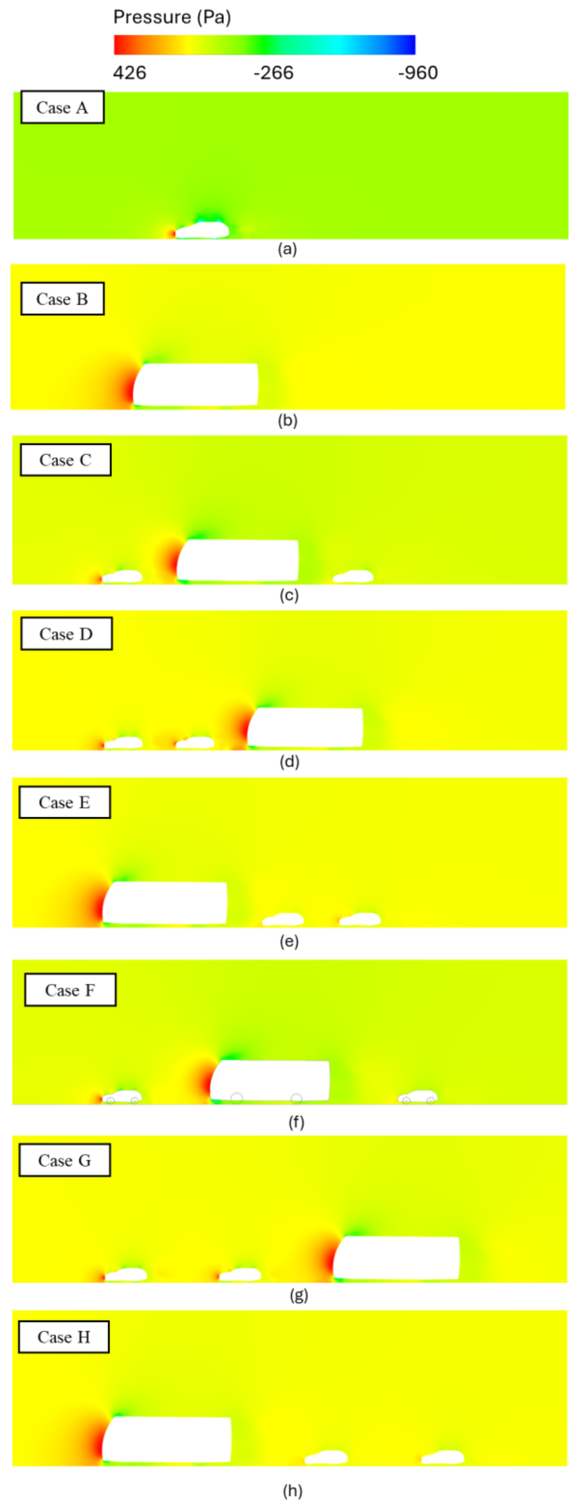

Fig. 10 Pressure contour for Case A, Case B, Case C, Case D, Case E, Case F, Case G and Case H

In Case E, the bus at the front generates a substantial high-pressure region and a large wake that affects both trailing cars. Although the 4-meter spacing allows for some airflow recovery, the trailing cars are still impacted by the bus's wake, reducing their aerodynamic efficiency. The 8-meter spacing in Case F improves airflow between the vehicles, decreasing wake interference and stabilizing the pressure gradients around the trailing car. Case G demonstrates a more effective dissipation of the wakes produced by the two leading vehicles, allowing the bus to maintain a stable high-pressure zone at its front with reduced turbulence in the downstream flow. In Case H, the bus at the front creates a significant wake that affects the first trailing car. However, the 8-meter spacing enables the second trailing car to experience smoother pressure gradients, enhancing its aerodynamic performance. The increased longitudinal spacings seen in Cases F–H showcase notable benefits in minimizing wake effects and improving overall stability.

The 3D vortex formations in Fig. 11 highlight how vehicle configuration and spacing affect wake dynamics. In Case C, the bus's central position creates a large turbulent vortex around the trailing car, with minimal airflow recovery due to a 4-meter spacing, resulting in chaotic flow and increased instability. Case D merges wake vortices from both leading vehicles, leading to a complex and turbulent vortex system. In Case E, the bus generates a dominant 3D vortex affecting both trailing cars, with limited airflow recovery causing unstable vortices and increased drag. Case F benefits from an 8-meter longitudinal space, improving spacing and airflow recovery, resulting in smoother vortex transitions for the trailing car. Case G sees greater vehicle separation, allowing distinct wake structures to dissipate before interacting with the bus, leading to more organized vortex patterns despite the bus's dominating wake. In Case H, the leading bus strongly affects the first trailing car while minimizing interference for the second, enhancing flow stability.

Overall, the results illustrate that 4-meter gaps lead to turbulent and chaotic vortex formations (Cases C, D, and E), while 8-meter spacings enhance stability and reduce drag (Cases F, G, and H). Central positions exacerbate wake disturbances, whereas rear positions stabilize upstream vehicles..

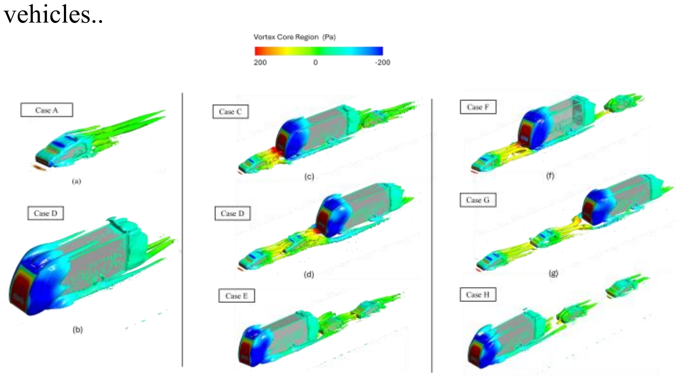

Fig. 11 *3D vortex for Case A, Case B, Case C, Case D, Case E, Case F, Case G and Case H*

B. *Aerodynamic forces*

This section analyzes aerodynamic forces on a double-decker bus compared to a car, focusing on vehicle positions and longitudinal spacings. Fig. 12 shows drag coefficients (C_d) for various configurations: (a) Cases C and F, (b) Cases D and G, and (c) Cases E and H. In the Car-Bus-Car arrangement (Fig. 12 (a)), Case C with a 4-meter longitudinal space shows the leading car's C_d at 0.381, the bus at 0.681, and the trailing car at 0.267. With an 8-meter spacing in Case F, the leading car's C_d drops to 0.239 and the trailing car's to 0.249, while the bus's C_d stays stable at 0.688. In the Car-Car-Bus configuration (Fig. 12 (b)), Case D with a 4-meter spacing has the leading car at 0.3692, the middle car benefiting from the wake at 0.2608, and the bus at 0.66. At an 8-meter spacing in Case G, the leading car's C_d increases to 0.437, and the middle car's to 0.34, with the bus's drag slightly rising to 0.687. In the Bus-Car-Car arrangement (Fig. 12 (c)), Case E at 4 meters places the bus at the front with a C_d of 0.671, allowing the first trailing car to have a C_d of 0.148. At 8 meters in Case H, the bus's drag decreases to 0.669, while the first trailing car's C_d rises to 0.226, and the second drops to 0.212 due to improved airflow.

At 4-meter spacings, closer spacing reduces drag for trailing cars via wake shielding, while 8-meter spacings enhance airflow recovery, redistributing aerodynamic forces to lower drag on the second trailing car and slightly increasing it for the first. The bus's position is crucial, as leading buses generate significant drag and influence downstream flow dynamics.

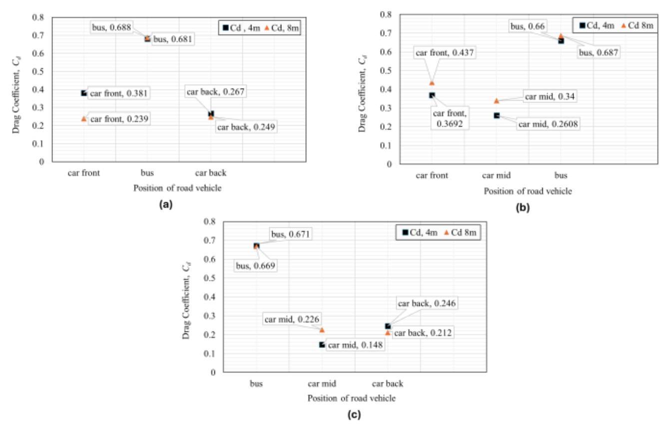

Fig. 12 Drag Coefficient, C_d, for different road positions. (a) Case C and F, (b) Case D and G, (c) Case E and H

Fig. 13 presents the lift coefficients (C_l) for different vehicle configurations at various longitudinal spacings. In Case C, with a 4-meter spacing, the leading car (Car Front) has a lift coefficient of 0.29. Meanwhile, the bus exhibits a slightly negative coefficient of -0.0962 due to significant downwash, and the trailing car (Car Back) registers a value of 0.266, influenced by the turbulent wake from the bus. In Case F, with an 8-meter spacing, the lift of the leading car decreases to 0.179, while the bus's coefficient slightly drops to -0.0809. In this case, the lift of the trailing car rises to 0.375, benefiting from reduced wake interference. In Case D, with a 4-meter spacing, the leading car (Car Front) maintains a lift coefficient (C_l) of 0.314, while the middle car (Car Mid) has a lower value of 0.242, and the bus at the rear shows a lift coefficient (C_l) close to zero of 0.00391. For Case G, at an 8-meter spacing, the leading vehicle's lift increases to 0.34, the lift of the middle car decreases to 0.192, and the bus experiences a negative lift coefficient (C_l) of -0.0923 due to less turbulence and improved downwash. With a 4-meter spacing, the bus generates considerable downward forces in Case E, reflected in a lift coefficient (C_l) of -0.167. The first trailing car (Car Mid) experiences a lift of 0.255, while the second trailing car (Car Back) registers a lift of 0.0776. In Case H, with an 8-meter spacing, the bus's lift remains relatively unchanged at -0.173, the lift of the first trailing car decreases to 0.205, and the second trailing car's lift increases to 0.102, thanks to smoother airflow. Overall, lift coefficients (C_l) were influenced by longitudinal spacings and the positions of the vehicles. At a 4-meter spacing, closer spacing enhances lift for trailing cars while reducing it for the bus. In contrast, at an 8-meter spacing, the lift distribution becomes more balanced, with reduced wake interference leading to improved lift for trailing vehicles and lower lift for the bus and leading cars.

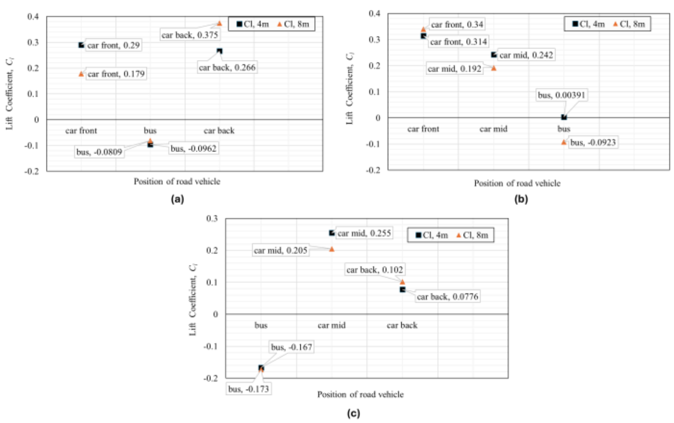

Fig 13 Lift coefficient, C_l, for different road positions. (a) Case C and F, (b) Case D and G, (c) Case E and H

C. Aeroacoustics analysis

Fig. 14 presents the acoustic power levels for Cases C, D, E, F, G, and H. In Case C Fig. 13(a), moderate acoustic power (16-33 dB) is found at the rear of the bus due to wake turbulence and trailing car interactions, while the cars also show moderate power from turbulent airflows. The blue area on the bus's roof indicates higher levels (49-65 dB) linked to complex turbulence patterns from its large, boxy shape. In Case D, yellow-green regions at the bus's rear signify significant noise from wake turbulence, with the cars showing light green to yellow areas reflecting moderate power due to flow separation. The blue zones over the bus roof again indicate the highest acoustic power from vortex interactions.

In Case F as shown in Fig. 14(d), with an 8-meter spacing, acoustic power levels decrease compared to Case C, with light green regions around the bus's rear indicating moderate noise and blue regions over the roof indicating high levels (49-65 dB) from residual disturbances. The cars show yellow-green regions, reflecting reduced turbulence due to larger spacing. In Case G, yellow-green regions signify moderate power (16-33 dB) at the bus's rear, while the cars exhibit green regions from wake interactions, and blue areas over the roof represent the highest power levels. Fig. 14(f) for case H, the bus generates the highest acoustic power, with yellow-green regions at its rear and blue zones over the roof due to turbulent interactions. The cars, positioned further away, display light green to blue regions indicating lower power from dissipated turbulence. Overall, acoustic power levels are affected by vehicle spacing, with larger spacings resulting in reduced turbulence and noise, particularly near the bus's roof and rear, while trailing cars experience less noise due to increased spacing.

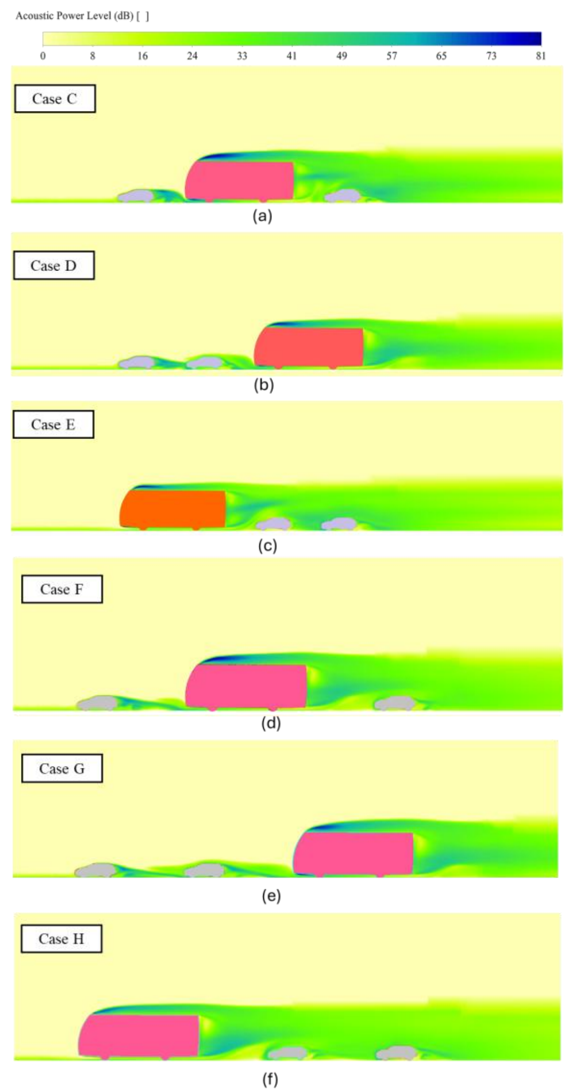

Fig. 14 Acoustic Power for Case C, Case D, Case E, Case F, Case G and Case H

Figure 15 showcases the surface acoustic power for Cases C, D, and E, all featuring a 4-meter longitudinal space. In Case C, illustrated in Fig. 15(a), the bus demonstrates moderate acoustic power levels ranging from 35 to 53 dB along its sides and rear, indicating the presence of wake turbulence, while the cars positioned in front and behind exhibit blue-green areas that reflect their interaction with the bus's wake, leading to increased turbulence and noise due to their close proximity. In Case D, shown in Fig. 15(b), the acoustic power distribution shifts slightly, with the bus still displaying dominant green regions and the cars revealing yellow zones at their rear, pointing to the combined effects of the trailing bus and adjacent vehicles, resulting in a more uniform turbulence without extreme high-power zones. Case E maintains the bus's green zones but shows more pronounced yellow regions at the rear of the cars, indicating higher turbulence due to the bus's leading position, which underscores the significant impact of the bus's placement on the aeroacoustics behaviour of surrounding vehicles.

In Cases F, G, and H, which use an 8-meter longitudinal space, acoustic power is notably reduced; in Case F, shown in Fig. 15(d), the bus features green regions with minimal yellow zones, suggesting less wake turbulence and smoother airflow, while the cars display faint yellow-green areas due to increased spacing. Case G continues this trend with further reductions in turbulence-induced noise, and in Case H, illustrated in Fig. 15(f), the bus exhibits light green zones indicating minimal wake turbulence, while the cars present faint yellow-green regions due to residual turbulence, highlighting the effectiveness of larger longitudinal spacings in reducing aeroacoustic noise levels. Overall, these findings illustrate that increasing the longitudinal space effectively reduces wake interactions, resulting in lower acoustic power levels and quieter vehicle configurations.

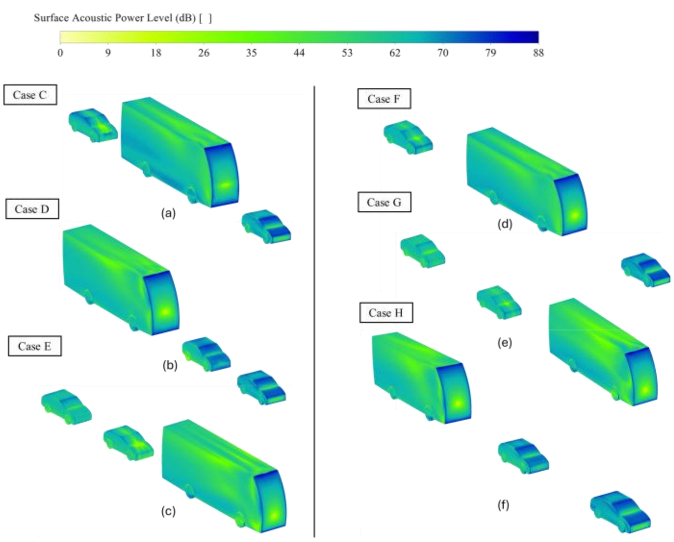

Fig. 15 Surface Acoustic Power for Case C, Case D, Case E, Case F, Case G and Case H

IV. CONCLUSION

This study utilized computational fluid dynamics (CFD) to map the aerodynamic and aeroacoustic interactions across various mixed-vehicle platoons. The simulations confirm that both the sequence of vehicles and the distance between them fundamentally dictate wake vortex structures, surface pressure, and acoustic power generation. We found that the Bus-Car-Car sequence with a 4 m gap offers the greatest aerodynamic benefits. In this setup, the lead bus experienced a 37% drop in its drag coefficient, while the trailing cars saw massive drag reductions of 50–60%. These drops translate directly to improved energy efficiency and vehicle stability. Furthermore, expanding the longitudinal spacing further reduced surface noise and smoothed aerodynamic drag across all trailing vehicles. Ultimately, strategically organizing multi-vehicle systems can drastically cut fuel consumption and emissions. Future work should transition these numerical models into experimental and dynamic road testing to fully bridge the gap between CFD simulations and real-world sustainable transportation.

ACKNOWLEDGMENT

Communication of this research is made possible through monetary assistance from Universiti Tun Hussein Onn Malaysia.

AUTHOR CONTRIBUTIONS

The authors confirm their contributions to the paper as follows: study conception and design: Nur Rasyidah Roziman, Izuan Amin Ishak, Mohammad Arafat, Nor Afzanizam Samiran; data collection: Nur Rasyidah Roziman; analysis and interpretation of results: Nur Rasyidah Roziman, Nur Haziqah Shaharuddin, Mohammad Arafat, Fadhilah Mohd Sakri; draft manuscript preparation: Nur Rasyidah Roziman, Izuan Amin Ishak, Muhammad Aidil Safwan Abdul Aziz, Muhammad Nabil Farhan Kamal. All authors reviewed the results and approved the final version of the manuscript.

AI TOOL USAGE ACKNOWLEDGMENT

The author declares that no AI technology tools were utilised during the preparation and writing of this article. An AI-assisted tool was used solely to check English grammar and refine sentence structure.

CONFLICT OF INTEREST

The author declares that there is no conflict of interest regarding the publication of this article.

REFERENCES

[1] S. Hassan, H. A. Amlan, N. E. Alias, M. A. A. Kadir, N. Mashros, and N. S. A. Sukor, "Vulnerability of Road Transportation Networks: A Bibliometric Analysis," *SSRN Electron. J.*, 2022, doi: 10.2139/ssrn.4002940.

[2] W. J. Lee, S. Il Kwag, and Y. D. Ko, "The optimal eco-friendly platoon formation strategy for a heterogeneous fleet of vehicles," *Transp. Res. Part D Transp. Environ.*, vol. 90, p. 102664, Jan. 2021, doi: 10.1016/j.trd.2020.102664.

[3] M. Siemon and D. S. Nichols, "CFD analysis of heterogeneous and homogeneous multi-truck platoon aerodynamic drag reduction," *2018 Fluid Dyn. Conf.*, 2018, doi: 10.2514/6.2018-3862.

[4] S. T. Kaluva, A. Pathak, and A. Ongel, "Aerodynamic Drag Analysis of Autonomous Electric Vehicle Platoons," *Energies*, vol. 13, no. 15, p. 4028, Aug. 2020, doi: 10.3390/en13154028.

[5] V. Vohra, M. Wahba, G. Akarslan, R. Ni, and S. Brennan, "An Examination of Vehicle Spacing to Reduce Aerodynamic Drag in Truck Platoons," in *2018 IEEE Vehicle Power and Propulsion Conference (VPPC)*, IEEE, Aug. 2018, pp. 1–6. doi: 10.1109/VPPC.2018.8604977.

[6] F. H. Robertson *et al.*, "An experimental investigation of the aerodynamic flows created by lorries travelling in a long platoon," *J. Wind Eng. Ind. Aerodyn.*, vol. 193, p. 103966, Oct. 2019, doi: 10.1016/j.jweia.2019.103966.

[7] M. He *et al.*, "Detached eddy simulation of a closely running lorry platoon," *J. Wind Eng. Ind. Aerodyn.*, vol. 193, Oct. 2019, doi: 10.1016/j.jweia.2019.103956.

[8] W. M. Hamiga and W. B. Ciesielka, "Numerical Analysis of Aeroacoustic Phenomena Generated by Heterogeneous Column of Vehicles," *Energies*, vol. 15, no. 13, p. 4669, Jun. 2022, doi: 10.3390/en15134669.

[9] P. Qin, A. Ricci, and B. Blocken, "CFD simulation of aerodynamic forces on the DrivAer car model: Impact of computational parameters," *J. Wind Eng. Ind. Aerodyn.*, vol. 248, p. 105711, May

2024, doi: 10.1016/j.jweia.2024.105711.
[10] S. Wang, T. Avadiar, M. C. Thompson, and D. Burton, "Effect of moving ground on the aerodynamics of a generic automotive model: The DrivAer-Estate," *J. Wind Eng. Ind. Aerodyn.*, vol. 195, p. 104000, Dec. 2019, doi: 10.1016/j.jweia.2019.104000.
[11] M. Arafat *et al.*, "A Hybrid RANS/LES Model for Predicting the Aerodynamics of Small City Vehicles," *J. Adv. Res. Exp. Fluid Mech. Heat Transf.*, vol. 17, no. 1, pp. 1–13, Sep. 2024, doi: 10.37934/arefmht.17.1.113.
[12] J. Tu, G. H. Yeoh, C. Liu, and Y. Tao, "Practical Guidelines for CFD Simulation and Analysis," in *Computational Fluid Dynamics*, Elsevier, 2024, pp. 251–285. doi: 10.1016/B978-0-323-93938-6.00011-7.
[13] F. MENTER, "Performance of popular turbulence models for attached and separated adverse pressure gradient flows," in *22nd Fluid Dynamics, Plasma Dynamics and Lasers Conference*, Reston, Virigina: American Institute of Aeronautics and Astronautics, Jun. 1991. doi: 10.2514/6.1991-1784.
[14] L. Wang *et al.*, "Analysis of the Influence of Different Turbulence Models on the Prediction of Vehicle Aerodynamic Performance," *Energies*, vol. 18, no. 11, p. 2803, May 2025, doi: 10.3390/en18112803.
[15] M. Syafiq *et al.*, "Computational Fluid Dynamics Analysis of Aerodynamic Characteristics on Overtaking Vehicles in Crosswind Conditions," *Int. J. Automot. Mech. Eng.*, vol. 22, no. 2, pp. 12373–12387, Jun. 2025, doi: 10.15282/ijame.22.2.2025.10.0947.
[16] R. F. Soares, K. P. Garry, and J. Holt, "Comparison of the Far-Field Aerodynamic Wake Development for Three DrivAer Model Configurations using a Cost-Effective RANS Simulation," in *SAE Technical Papers*, Mar. 2017. doi: 10.4271/2017-01-1514.
[17] F. Delassaux, V. Herbert, I. Mortazavi, and C. Ribes, "Numerical Investigation of the Flow Around a Simplified Ground Vehicles Using Hybrid RANS/LES Method," in *Notes on Numerical Fluid Mechanics and Multidisciplinary Design*, vol. 143, 2020, pp. 357–365. doi: 10.1007/978-3-030-27607-2_29.

Nur Rasyidah Roziman is currently pursuing a Bachelor of Mechanical Engineering Technology (Automotive) with Honours at Universiti Tun Hussein Onn Malaysia, Muar, Johor. Her research interests include computational fluid dynamics (CFD) simulation analysis using SolidWorks and ANSYS software, as well as automotive engineering technology. She has actively contributed to academic and extracurricular activities, serving as a Committee Member of the Automotive Engineering Technology Club (Autobot) and the CFD Community. Ms. Roziman's achievements include receiving the Gold Award at the Semarak International Research Article Competition 2024 II (SIRAC 2024 II). She also holds a certificate of competency in SolidWorks: Fundamentals of Design and Validation Course.

Izuan Amin Ishak was born in Georgetown, Penang, Malaysia, in 1985. He received his Master of Engineering (MEng) degree in Mechanical Engineering from the University of Manchester, UK, in 2009 and his PhD degree in Mechanical Engineering from Universiti Teknologi Malaysia (UTM) in 2018. From 2009 to 2014, he worked as a research and development engineer at Perodua Manufacturing Sdn. Bhd., where he was responsible for the development of external lamp parts until their mass production. In 2017, he joined UniKL Malaysian Institute of Aviation Technology (MIAT) as a lecturer. Since 2018, he has been a Senior Lecturer at the Mechanical Engineering Technology Department, Universiti Tun Hussein Onn Malaysia, Pagoh Campus. He is also a member of the Board of Engineers Malaysia (BEM) and a professional technologist of the Malaysia Board of Technologists (MBOT). His research interests include those involved with fluid flow analysis through computational fluid dynamics (CFD). Currently, his research is focusing on vehicle aerodynamics, energy harvesting through wind engineering, and bio-inspired propeller design. At UTHM, he is a principal researcher at the Centre of Automotive & Powertrain Technology (CAPT) and an associate researcher at the Industry Centre of Excellence for Railway (ICOE-REL). He has secured more than 15 grants, totalling over RM 400,000, as a principal investigator and team member from university and national-level grants to support his research. In terms of research papers, he has published over 20 peer-reviewed journal articles and conference papers. He is also a regular reviewer for several international journals and conferences.

Mohammad Arafat is a prominent researcher specializing in aerodynamics, computational fluid dynamics (CFD), and aeroacoustics. He holds a PhD from Universiti Tun Hussein Onn Malaysia (UTHM), where his doctoral work focused on high-fidelity CFD simulations of bio-inspired UAV propellers to optimize aerodynamic performance and reduce noise generation. Dr. Arafat also earned a Master of Engineering Technology from UTHM specializing in high-speed train crosswind aerodynamics and a bachelor's degree in industrial engineering from Telkom University. An accomplished academic, he has authored over 30 peer-reviewed journal articles and book chapters indexed in Web of Science (WoS) and Scopus. Dr. Arafat is currently working as a Postdoctoral Researcher at the Malaysian Institute of Aviation Technology (UniKL MIAT), where he bridges advanced numerical simulations with experimental wind-tunnel testing, structural analysis, and psychoacoustic assessments. He is also a recipient of multiple international research awards, an undergraduate mentor, and a specialized technical trainer who has upskilled university lecturers in ANSYS, StarCCM+, and MATLAB.

Nor Afzanizam Samiran was born in Batu Pahat, Johor, Malaysia, in 1986. He obtained his Bachelor's Degree in Mechanical Engineering (with Honours) in 2009 from the Universiti Kebangsaan Malaysia (UKM), a Master's Degree in Mechanical Engineering from the Universiti Tun Hussein Onn Malaysia (UTHM) in 2012, and a Doctor of Philosophy in Mechanical Engineering from Universiti Teknologi Malaysia (UTM) in 2017. He worked as a production engineer at Kiswire Sdn. Bhd. And Guocera Tiles Industries Sdn. Bhd. from 2009 to 2011, where he was responsible for managing the manufacturing production system and product quality control. Since 2017, he has been a senior lecturer in the Mechanical Engineering Technology Department at Universiti

Tun Hussein Onn Malaysia. He is a registered member of the Board of Engineers Malaysia (BEM) and the Malaysia Board of Technologies (MBOT). He is also qualified to be certified as a Safety and Health Officer by the National Institute of Occupational Safety and Health (NIOSH). He also obtained competence certification from Autodesk as an AutoCAD Professional Trainer. His research interests are in the field of renewable energy, with a specific interest in waste management and fuel production technology, combustion, and gasification reaction mechanisms, experimental studies on the performance of gas-fuelled boiler/gas turbine engines and solid gasification reactors, CFD simulation of renewable energy, including clean fuel and aerodynamics of the wind turbine. He is a principal researcher for the focus group of Integrated Engineering Simulation Design (IESD) and Combustion Research Group (CRG). He has secured 20 research grants as a project leader and team member with more than RM200,000 at the University, national, and industrial levels. In addition, he has published more than 15 peer-reviewed journal articles and conference papers. He also serves as a reviewer for more than 20 WOS/ISI-indexed journals.

Nur Haziqah Shaharuddin is currently pursuing her Ph.D. at Keio University, Japan, with a research focus on fluid mechanics, computational fluid dynamics (CFD), turbulence modelling and aerodynamic noise. Her research involves advanced numerical simulations to analyse complex fluid flow phenomena, particularly in aerodynamic and industrial applications.

Fadhilah Mohd Sakri was born in Malaysia in 1989. She obtained her Master’s Degree in Aircraft Design Engineering from Moscow Aviation Institute (MAI) – National Research University, Russia, in 2014, and her Doctor of Philosophy in Mechanical Engineering from Universiti Teknologi Malaysia (UTM) in 2017. She is currently a Senior Lecturer II at Taylor's University, Malaysia. She is a Graduate Engineer with the Board of Engineers Malaysia (BEM) and a member of the Institution of Engineers Malaysia (IEM) and the World Academy of Research in Science and Engineering. Her research interests include computational fluid dynamics (CFD), aerodynamics, fluid mechanics, and heat transfer. She has been actively involved in various research and industrial projects, particularly in CFD analysis for aircraft, unmanned aerial vehicles (UAVs), and aerodynamic performance studies. She has published numerous journal articles and conference papers, served as a reviewer for international journals, and secured multiple research grants as both a project leader and a team member.

Muhammad Aidil Safwan Abdul Aziz is currently pursuing his Doctor of Philosophy (PhD) at the Faculty of Engineering Technology (FTK), Universiti Tun Hussein Onn Malaysia (UTHM), Kampus Pagoh, Muar, Johor. Building directly upon his postgraduate research foundations, his current PhD interests center on advanced computational fluid dynamics (CFD) simulation analysis, innovative fluid mechanics, and the thermal performance optimization of engineering systems. His master's research focused heavily on electronics device cooling systems and microchannel heat sinks. He remains actively involved within the faculty's specialized engineering communities, aiming to bridge the gap between experimental numerical analysis and real-world mechanical applications.

Muhammad Nabil Farhan Kamal was born in Malaysia. He graduated with a Bachelor's Degree in Mechanical Engineering from Universiti Tun Hussein Onn Malaysia (UTHM) in 2020. He is currently a project engineer at Pentamaster, Malaysia, where he is involved in engineering solutions for advanced manufacturing and industrial processes. He is a registered Engineering Technologist with the Board of Engineers Malaysia (BEM) and has professional certifications in Lean Six Sigma Green Belt, Statistical Process Control (SPC), Failure Analysis, Reliability Testing, and CATIA V5. His professional interests focus on automotive manufacturing, production engineering, quality improvement, engineering simulation, automation, and advanced manufacturing technologies. He has participated in various engineering and industrial projects related to manufacturing process optimization and product quality enhancement.